Propulsion Rig: A multirotor performance measurement test platform

Guy Hasewinkel[1*], *Arnold* Pretorius[1]

[1]MechatronicSystems.Group, Department of Mechanical Engineering, University of Cape Town, South Africa

Abstract. Off-the-shelf multirotor propulsion system components can produce uncertain static and dynamic performance. Commercially, solutions exist to characterise the inexact performance of the propulsion system, yet they are prohibitively expensive. To that end, the Propulsion Rig, a low-cost and open-source multirotor test platform, is developed and used to measure the principal performance characteristics of multirotor propulsion systems. The data gathered can be used to generate static and dynamic models of the propulsion system of interest, thereby reducing the uncertainty in the drivetrain performance. The models can be used to validate conceptual multirotor designs, and, additionally, incorporated into simulation models to aid the control design process. By accounting for the propulsion system dynamics, the control scheme performance can potentially be improved. Static propeller characterisation results obtained from the Propulsion Rig are shown to closely match data provided in reputable online databases.

1 Introduction and background

Unmanned Aerial Vehicles (UAVs) have become ubiquitous in their application and have seen a significant increase in research into the technology. Multirotor Aerial Vehicles (MRAVs), commonly known as drones, are being used in an ever-increasing variety of tasks in the real world. However, the constituent components of the multirotor drivetrain generally stem from off-the-shelf parts. Brushless DC motors, propellers, and electronic speed controllers, in various combinations, produce wide ranging and, at times, uncertain static and dynamic performance, which makes conceptual design non-trivial. To account for this, the propulsion system operating conditions can be emulated in an environment of sensors that capture the fundamental performance characteristics.

There have been numerous systems built for the purpose of characterising a propulsion system. These systems have been built within commercial, research and hobbyist domains. Generally, hobbyist solutions are cost-effective, but only measure thrust, while commercial solutions are usually expensive, but measure torque too; research solutions fall somewhere between. There are two prominent commercially available solutions, namely those from Tyto Robotics and Wing Flying Tech, as seen in Fig. 1. The most affordable products offered by the two companies, and most applicable for small to medium scale MRAVs, cost $1075

* Corresponding author: HSWGUY001@myuct.ac.za

(R19 957) and $2669 (R48 575), respectively [1-2]. This price point can be an infeasible cost for research institutes with limited funding. Both products are machined from high strength metal and use a simple parallel beam load cell setup to measure thrust and torque. Additionally, both companies provide an accompanying graphical user interface (GUI) that automates the testing and data capture process. Furthermore, the two solutions sense a range of quantities, such as thrust, torque, current, and rotational angular velocity. The performance specifications are summarised in Table 1.

Fig. 1. Left: Series 1585 Thrust Stand by Tyto Robotics [1]. Right: LY-10KGF Thrust Stand by Wing Flying Technologies [3]

Table 1. Specifications of the Series 1585 Thrust Stand by Tyto Robotics and the LY-10KGF Thrust Stand by Wing Flying Technologies [1-2]

Specification	Tyto Robotics Series 1585 Thrust Stand	LY-10KGF Thrust Stand by Wing Flying Technologies
Maximum sensed thrust	5 kgf	10 kgf
Maximum sensed torque	2 Nm	5 Nm
Maximum operating voltage	50 V	65 V
Measurement sampling rate	80 Hz	Not specified

The reported research and hobbyist solutions, to varying extents, lack the necessary characteristics to either replicate or perform high fidelity system identification on propulsion systems in a low-cost manner. Neto, Brezina et al., and Buzzatto et al. all effectively characterise propulsion systems through the fabrication of purpose-built rigs to differing degrees [4-6]. Neto implements a non-static design using a combination of t-slot extrusions to actuate the load cells. Their approach, however, is vulnerable to noise in the load cell measurements and makes use of costly transducers [4, 7]. Brezina et al., on the other hand, implements a stationery arrangement, but this comes at the expense of using a torque sensor amounting to $1115 (R19 743) [5, 8]. Lastly, Buzzatto uses the simplest configuration of the three, but utilises a NI myRIO device amounting to $937 (R16 624) to route their sensor suite signals [6, 9]. Additionally, none of the three solutions are made openly available [4-6]. In contrast, Bartnick, designed a fully 3D printable solution that is open source, yet neglects several critical measurands, such as current and rotor angular velocity [10].

Due to the lack of low-cost and replicable solutions, the aim of this project is to develop an open-source measurement system with similar functional performance characteristics to those of the commercially available counterparts. By doing so, the data from the sensor suite of the measurement rig can be used to model the static and dynamic behaviour of the propulsion system of interest. The generated models allow for the conceptual multirotor design to be validated and iterated upon, which aids in component selection for the particular multirotor use case. Additionally, the insights gained from the dynamic models can be incorporated into the model-based simulation and control design of the multirotor, thereby potentially improving the multirotor's performance and stability.

2 Methodology

The documented commercial, academic, and hobbyist solutions give an indication to the degree of fidelity that a propulsion system's characteristics can be measured. Through an examination of the reported approaches, a set of realistic and permissible attributes for the designed rig are generated as part of a user needs analysis. The user needs analysis informs the design process, ensuring quantifiable goals are met.

2.1 Abridged user requirement specifications

The abridged subset of user requirement specifications (URS) for the platform, informed by the user needs analysis, is given below.

Budget:

B1. The minimum viable platform shall cost less than R2500.00.

Constraints:

C1. The platform shall be applicable for propulsion system propellers between 5" (0.127 m) and 15" (0.381 m), with no limit on propeller pitch size.
C2. The platform shall be applicable for motors with an outer casing diameter between 10 mm and 30 mm.
C3. The platform shall be applicable for motors with an outer casing height between 15 mm and 50 mm.
C4. The platform shall mount the rotor and propeller unit perpendicular for any mounting surface.

Features:

F1. The platform shall measure thrust, current, propeller angular velocity, and commanded pulse-width-modulated (PWM) duty cycle.
F2. The platform(s) shall be configurable to measure propulsion systems in a coaxial arrangement.
F3. The platform's embedded system shall be able to record and save all measurements into a CSV file located within the local machine directory.

Performance:

P1. The measurement sampling rate of the platform's sensor suite shall be at least 80 Hz.
P2. The maximum measurable thrust of the platform shall be at least 3 kg.
P3. The maximum measurable current of the platform shall be at least 30 A.
P4. The maximum measurable rotor unit angular velocity shall be at least 20 000 RPM.

Safety and ergonomics:

E1. No component within the platform shall permanently deform during a testing procedure.

E2. The platform shall possess a mechanism that immediately terminates the testing procedure.

2.2 Mechanical design

Given the subset of the URS items scoped in Section 2.1, the principles followed during the rapid design iteration process were:

- Utilise the minimum number of components in the assembly of the rig,
- Minimise the machining of parts,
- Utilise the greatest number of commercially-off-the-shelf parts (COTS) (subject to cost),
- High sensing fidelity,
- Sensing simplicity.

The platform underwent numerous design iterations. The latest iteration, and the version that is open-sourced, can be seen in Fig. 2.

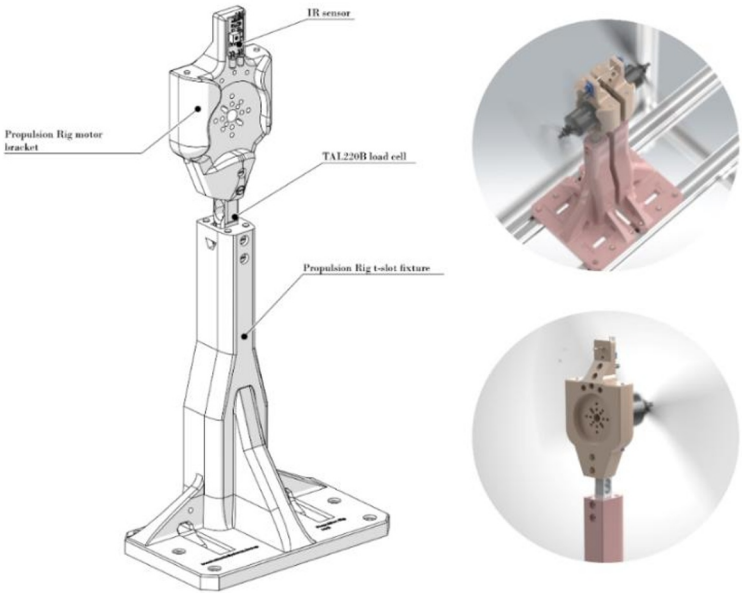

Fig. 2. Left: Annotated theoretical design render of the prototype measurement rig. Right: Photorealistic renders of the measurement rig in use in singular and coaxial configuration

The Propulsion Rig's design principle is simple; it uses a straight beam load cell in cantilever configuration, where one end is fixed, and on the other end, the thrust load is applied. The rig is primarily formed from two components, labelled as the bracket and the fixture in Fig. 2 and Fig. 3. The bracket mounts the rotor unit and load cell, while the fixture is fastened to two T-slot railings on its base, and on its opposite end, mounts to the load cell, as seen in Fig. 3. Two high-strength steel dowel rods can be inserted longitudinally into both the bracket and fixture to increase both components' strength properties. The load cell cantilever mechanism is formed through the fixed fixture, and free bracket. When the propeller generates thrust, a moment is induced on the straight bar beam load cell. The load cell is in full Wheatstone configuration, thus negating any strain that would otherwise be detected from the generated drag torque by the propellers. The bending moment results in elastic deformation, which in turn is captured by the resistors within the Wheatstone bridge of the load cell. The design principle can be seen in Fig 3.

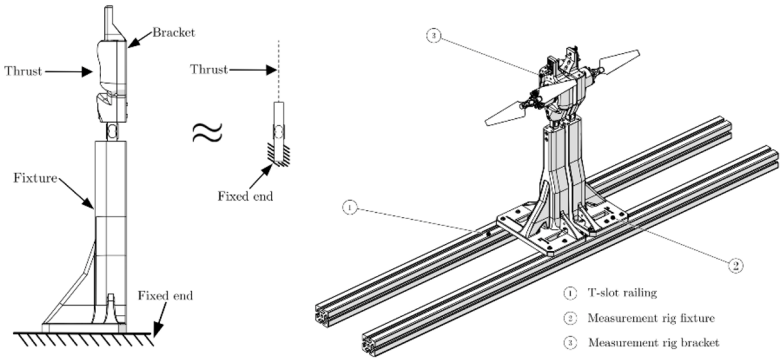

Fig. 3. Left: Thrust measurement principle on the measurement rig. Right: Measurement rig assembly in coaxial configuration mounted on two t-slot railings allowing for variable rotor-to-rotor spacing

The measurement rig went through several screening steps to refine the design's manufacturing quality, while maintaining a low-cost approach. The primary focus of each design step was to maximise the strength of the parts, and to minimise the associated drag. If the 3D-printed parts have insufficient strength, or non-negligible drag, the thrust production is adversely affected due to deformation in the 3D-printed part and obstructed airflow, respectively. Moreover, a yielding 3D printed part can break, posing a safety risk due to the kinetic energy of the spinning rotor unit, and the power draw from the motor. To ensure worthy trade-offs are made with respect to strength and drag characteristics of the 3D printed parts, SOLIDWORKS Simulation and SOLIDWORKS Flow Simulation were utilised [11-12]. Given the complexity in the strength modelling of 3D-printed parts, deformation simulations were conducted on three design iterations, shown in Fig. 4, with the results being compared to the respective baseline parts. Likewise, the aerodynamic characteristics of each part was evaluated by comparing each design iteration to the baseline parts. The numerical outcomes of the deformation and aerodynamic comparative analyses validated and guided the design direction. The final design iteration was affirmed by benchmarking a propeller's performance with the measurement rig, and then comparing the results to reputable data, as further explored in Section 3.1.

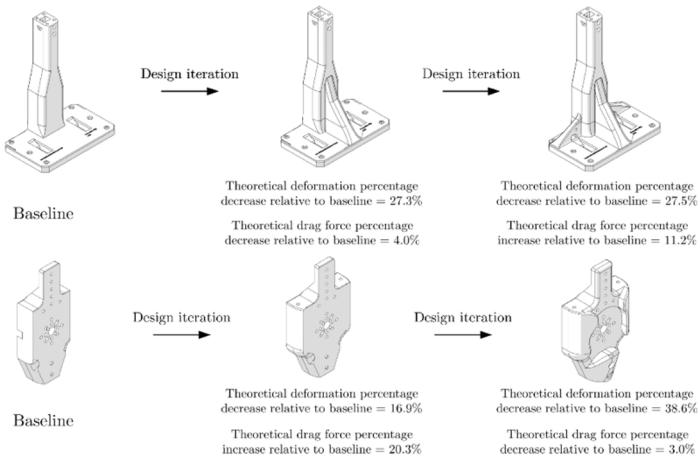

Fig. 4. Measurement rig design iteration renders with theoretical deformation and drag force comparative analyses results for the measurement rig fixture and bracket components to affirm and guide the design direction

2.3 Manufacturing

The Propulsion Rig's primary components are manufactured through additive manufacturing, namely fused filament fabrication, or 3D printing. 3D printing was chosen due to the degree of shape complexity it allows for, the minimal manufacturing cost, manufacturing accessibility and the low production time. Other manufacturing techniques, such as machining from suitable metals like aluminium, would improve the parts' strength characteristics, but would result in undesirable production costs and prototyping time. PLA is the chosen filament material, as it maximises both ultimate strength and stiffness, while being printable and relatively cost effective compared to other commercially available filaments. The 3D print settings for the bracket and fixture can be seen in Table 2.

Table 2. Propulsion Rig bracket and fixture 3D print settings

Configuration	Parameter
Wall loops	6
Top and bottom surface pattern	Hilbert curve
Sparse infill pattern	Gyroid
Sparse infill density	30%
Support	Tree (auto) is enabled on the bracket, and not enabled on the fixture

2.4 Embedded system design

The embedded system architecture is designed and implemented adhering to the items specified in Section 2.1 in the URS. Overall, the generated thrust, motor current draw, rotor angular velocity, and PWM commands are sensed, measured and recorded for later analysis. To do so, the embedded system architecture is structured around two separate microcontrollers. Specifically, two Arduino Uno's are used to simplify the data handling of incoming and outgoing signals through two respective serial channels. By doing so, the proposed approach negates any requirement on implementing code-based multithreading. On a top level, the measurement rig embedded system architecture is structured as shown in Fig. 5.

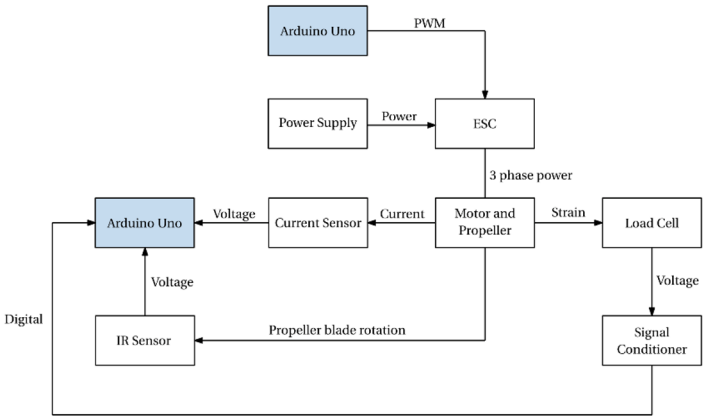

Fig. 5. Measurement rig embedded system architecture diagram

The measurement rig utilises an infra-red (IR) transmitter and receiver sensor to measure the propeller angular velocity [13]. The IR sensor toggles between logic HIGH voltage, and logic LOW voltage depending on whether there is an opaque object, like the propeller blade, in front of the beam area, or not. When the opaque propeller passes in front of the IR transmitted beam path, it reflects the incident infrared light back to the IR receiver. A potentiometer onboard of the IR sensor is used to refine the IR detection point for different pitch and diameter propellers, as each propeller has varying profiles that affect the efficacy of incidence. The configuration of the IR sensor on the measurement rig, along with the associated measuring principle, can be seen in Fig. 6. The rising edge of the IR sensor signal is used as a trigger within the microcontroller code to compute the angular velocity of the rotor unit within the interrupt service routine (ISR). The elapsed time between two rising edge trigger events generates the measured angular velocity of the rotor unit. The elapsed time between two ISR calls is determined through the ATMega328P's Timer 0 using the micros() function. The measured angular velocity updates with each iteration of the rising edge trigger event.

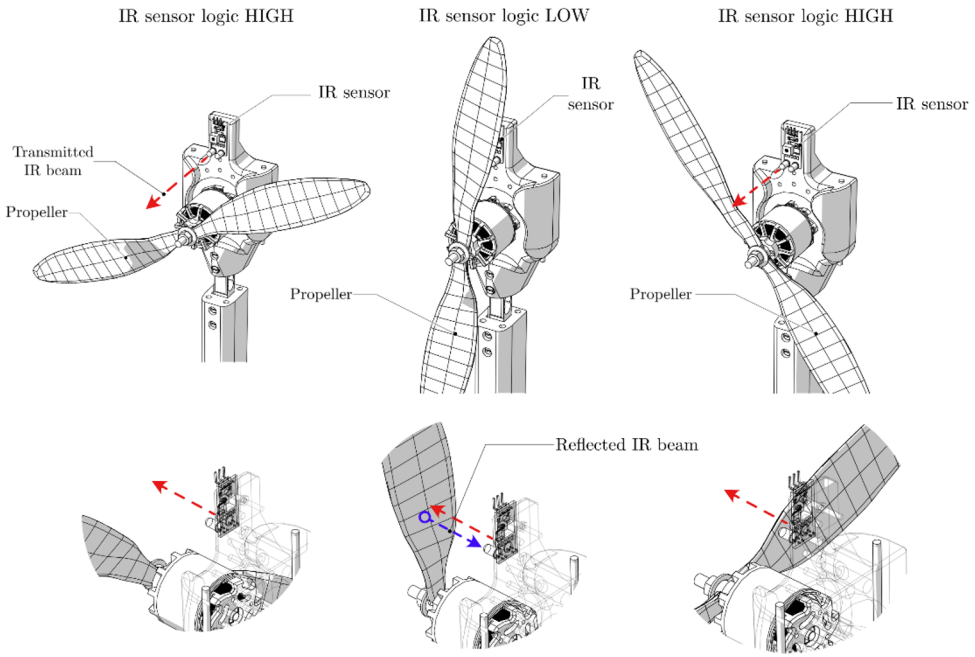

Fig. 6. Diagrammatic representation of the IR sensor configuration to sense the angular velocity of the rotor unit

The thrust and current are measured using readily available low-cost COTS parts. The current transducer is the AC758 hall effect sensor, and the thrust is measured using the parallel beam TAL220B load cell [14-15]. The load cell signal is amplified, and then discretised using the HX711, a low-cost COTS dual channel load cell amplifier and 24-bit ADC [15].

The embedded system code base is implemented on two microcontrollers, and one local PC machine. The testing routine is automated using a python script, whereby communication is routed through the respective serial ports of the microcontrollers. The python script performs the data acquisition process, along with implementing the user-defined testing

routine. Once a particular test is complete, the measured quantities are available within a timestamped CSV file for further analysis.

To evaluate a motor and propeller combination, there are two types of tests: static and dynamic. The static routine slowly ramps up and down from a minimum and maximum set PWM value. Each PWM value is maintained for a defined period of seconds to allow for the system dynamics to settle and reach a steady state value. Once the maximum PWM value is reached, the static routine inverts, and ramps down. The dynamic testing routine implements positive and negative step inputs at various starting values and step magnitudes. Both testing routine types can be seen in Fig 7.

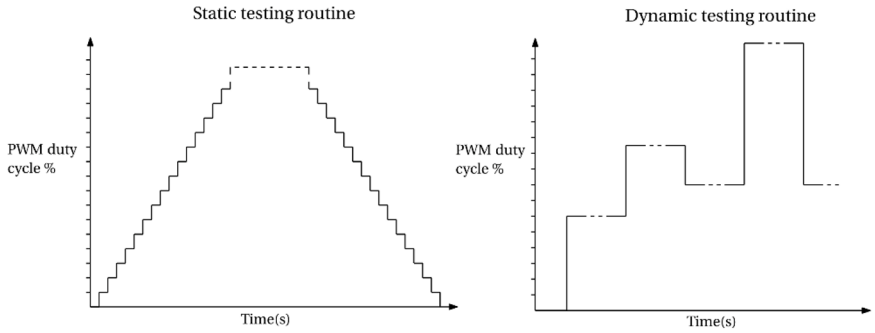

Fig. 7. Diagrammatic representation of the static and dynamic testing routines

The measurement rig components amount to under R1207, and the cost breakdown of the rig can be seen in Table 3. Development, manufacturing, and assembly costs are not considered, as they are variable and dependent on context.

Table 3. Breakdown of the associated measurement rig cost

Subsystem	Component	Quantity	Unit cost	Total cost
Hardware	Bracket	1	R43.26	R43.26
	Fixture	1	R143.31	R143.31
COTS hardware	Dowel rods	6	R15.30	R91.80
	T-slot railing	2	R53.40	R106.80
Embedded system	Arduino Unos	2	R149.00	R298.00
	Sensor suite	1	R416.05	R416.05
Total				R1206.02

3 Results

The successful fabrication and prototype of the designed measurement rig can be seen in Fig. 8. The prototyped rig fulfils all items scoped in the URS in Section 2.1. Specifically, the developed rig satisfies URS budget item B1, with each rig costing only R1207, 48% under the maximum permissible cost. Additionally, the measurement rig's mechanical dimensions comply with the URS' mechanical constraints, items C1 to C4, which are verifiable in the open-source design files. The prototyped embedded system and code base satisfy the required features specified in the URS, specifically F1 and F3. This is done by measuring and acquiring the thrust, current, propeller angular velocity, and commanded PWM duty cycle, which is shown in Section 2.4, and is illustrated in Section 3.1 and Section 3.2. Furthermore, two Propulsion Rigs can be mounted onto the T-slot railing back-to-back thus enabling coaxial testing, and meeting URS item F2. The transducers specified and the code base developed achieves the URS performance requirements, P1 to P4, which is observable in the open-source code base and test database. As evident in the successful acquisition of propulsion system data illustrated in Section 3.1 and Section 3.2, and additional extensive testing of the platform, the measurement rig achieves the safety and ergonomic URS requirements, E1 and E2.

Fig. 8. Fabricated measurement rig

The constituent components of the multirotor propulsion system produce wide-ranging and uncertain static and dynamic performance. To account for this, the embedded system measures, acquires, and conditions the following time-domain parameters: Thrust, motor current, rotor angular velocity, and PWM commands sent to the electronic speed controller (ESC). The collection of data is used to generate static and dynamic models of the propulsion system. A subset of example data is shown in Section 3.1 and Section 3.2 to illustrate the measurement rig's functionality, validity and use case.

3.1 Static tests

Statically testing the propulsion systems yield several useful parametric studies that give insight into the performance of the propeller and propulsion system, respectively. A small

subset of the relevant and useful parametric studies, and their purpose, can be seen in Table 4.

Table 4. Useful static performance parametric studies with use indicated

Static test parametric study	Purpose
Generated thrust versus angular velocity squared	Used to determine the propeller's coefficient of thrust and used to generate theoretical models
Generated thrust versus PWM duty cycle	Used to validate propulsion system performance and generate theoretical models
Motor current draw versus generated thrust	Used to validate propulsion system performance, indicate required battery specifications, and generate models

To determine and model the performance of the propeller with respect to the generated thrust and rotational velocity, a regression analysis can be performed on the acquired data. To illustrate the validity of acquired data from the measurement rig, an example comparative test is performed. In Fig. 9, publicly available data from the propeller manufacturer, APC propellers, is evaluated against that acquired by the measurement rig. Specifically, the parametric relationship between the generated thrust and associated angular velocity for APC's 10-inch diameter and 4.5-inch pitch multirotor propeller is explored. In Table 5, an error analysis is reported from the data presented in Fig. 9. The results indicate a systematic underestimation with the mean percentage error (MPE) being -9.13%. However, with both the mean absolute error (MAE) and root mean square error (RMSE) being less than 8.64 g and 9.60 g, respectively, the systematic underestimation is within an acceptable bound. The underestimation can be attributed to several factors, such as a degraded propeller, inaccurate taring and scaling of the load cell, drag effects from the measurement rig platform, and ground effect.

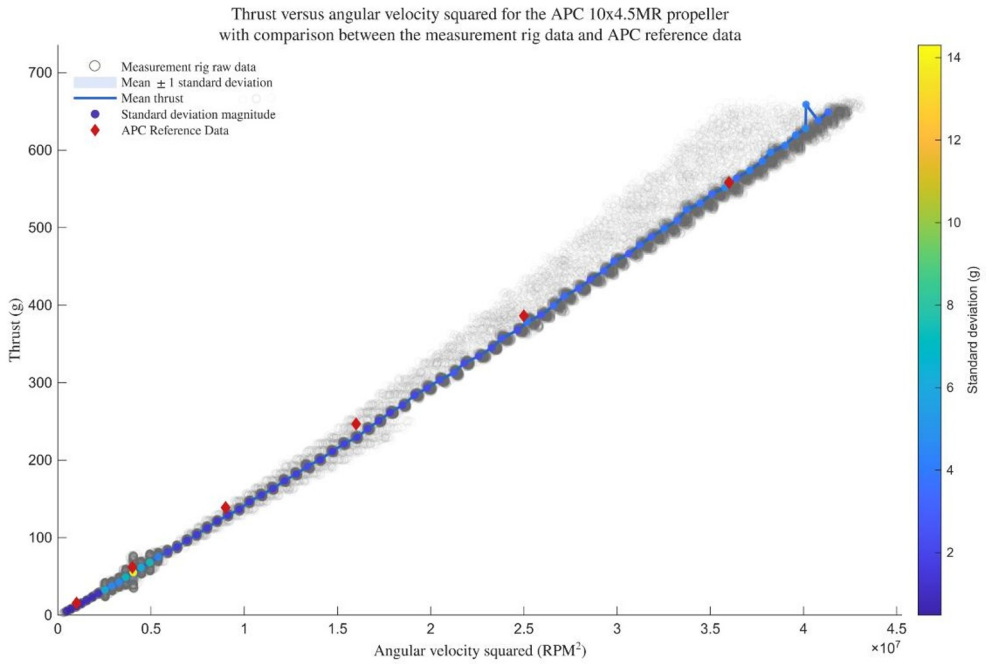

Fig. 9. Example comparison of the measured thrust and rotational from the measurement rig and data provided by the APC propeller manufacturers.

Table 5. Error analysis of the data presented in Fig. 9

Error analysis parameter	**MAE (g)**	**RMSE (g)**	**MPE (%)**
Value	8.64	9.60	-9.13

Using the same regression analysis shown in Fig. 9, the established method was extended to a varying set of unique APC propellers, as shown in Fig. 10.

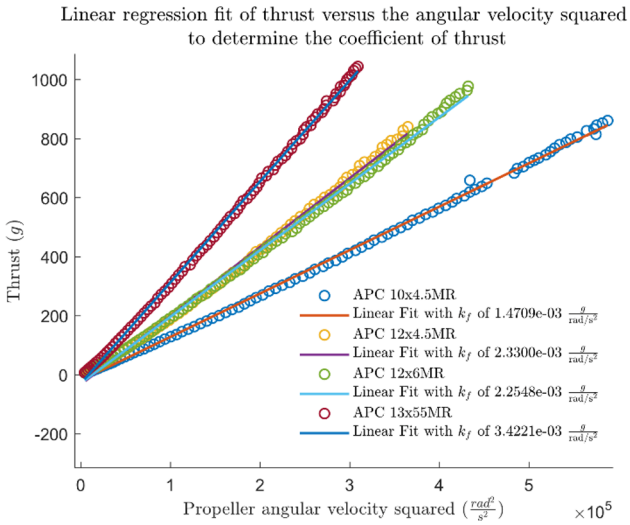

Fig. 10. Thrust versus the angular velocity squared for several varying APC propellers illustrating the differing propeller performance.

In addition to determining the propeller performance, an entire propulsion system can also be characterised using the measurement rig. For example, the T-motor AIR2216 880 Kv motor, with the T-motor T1045II propeller, and BLHeli 20 A ESC, produces the generated thrust given a commanded PWM duty cycle as shown in Fig. 11 when supplied with an operating voltage of 16 V. The generated third-order polynomial, indicated in Fig. 11, has an associated RMSE of 5.014 g and can be used to both validate the theoretical propulsion system design and be incorporated into the associated MRAV control scheme.

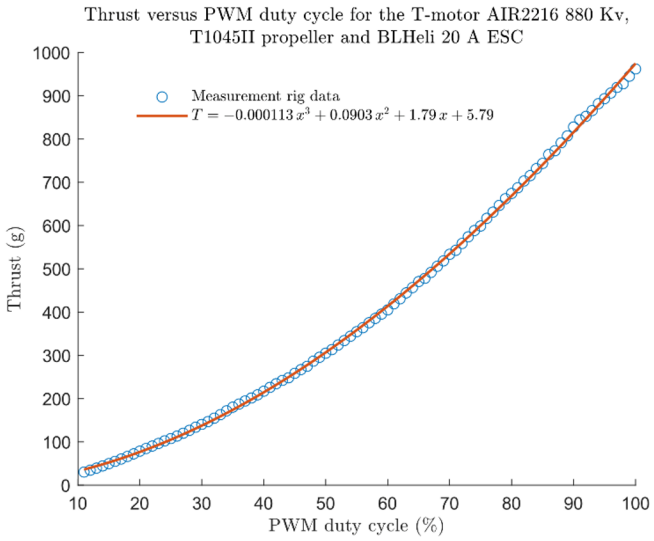

Fig. 11. Static response test of the Holybro X500 v2 propulsion system, parameterising the thrust and commanded PWM duty cycle response

In addition to parameterising the generated thrust given a commanded PWM duty cycle, a similar analysis can be performed to describe the relationship between the motor current draw and generated thrust. Given the same propulsion system indicated in Fig. 11, the motor current draw given a generated thrust is shown in Fig. 12. The generated second-order polynomial, overlayed in Fig. 12, has an associated RMSE of 0.306 A and can be used to both validate the theoretical propulsion system design and can be implemented into the associated MRAV control scheme.

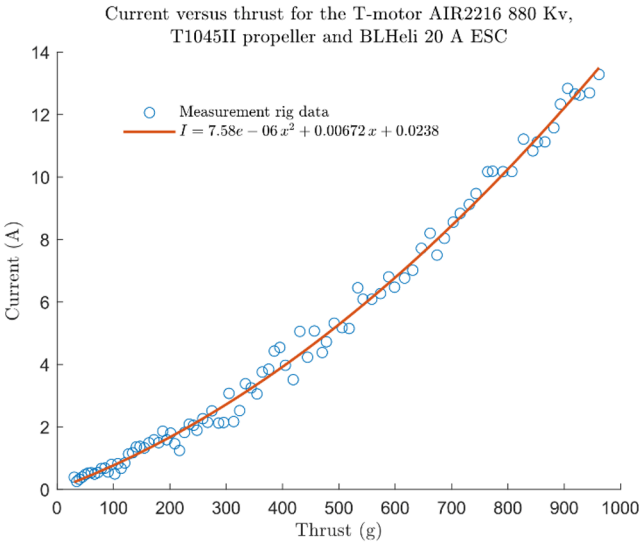

Fig. 12. Static response test of the Holybro X500 v2 propulsion system parameterising the current and thrust response.

3.2 Dynamic tests

When a rotor is commanded with a PWM duty cycle, the generated thrust response is composed of both transient and steady-state characteristics. It can be observed that the generated thrusts response, given a commanded PWM duty cycle, is suitably modelled as second order. The second order system assertion is supported through the experimentation and analysis of measured example data shown later in the section. The general second order dynamic response of the rotor system can be characterised in the Laplace domain by

$$P(s) = \frac{K\omega_n^2}{s^2 + 2\zeta\omega_n s + \omega_n^2} e^{-\tau s}, \tag{1}$$

where ω_n and ζ refer to the system's natural frequency and damping ratio, respectively, K is the steady-state value of the response, and τ is the system's time delay. The magnitude of these parametrised quantities inform the characteristics of the system's response.

The motor exhibits varying dynamic responses depending on the step thrust input initial value and final value. This is due to the non-linear relationship between the commanded PWM duty cycle and thrust, among other factors. To account for this, several dynamic response tests can be conducted at varying PWM step inputs. The models generated from the tests can then be stitched together to capture the entire permissible dynamic response range for the propulsion system. For each step command, the rotor's initial commanded PWM duty cycle and generated thrust are tared to ensure the removal of any residual dynamics.

The dynamic response of the same propulsion system used in Fig. 11 and Fig. 12 can be characterised using an arbitrary step-up and step-down input, as shown in Fig. 13. In Table 6, an error analysis of the generated second-order models from Fig. 13 are reported, where the step-up and step-down input models have a fit to estimation data of 97.9% and 94.4%, respectively, and an RMSE of 3.04 g and 7.96 g, respectively. Additionally, as reported in Table 6, there is a 128% and 106% increase in the damping ratio and natural frequency for the step-down test compared to the step-up test, respectively. As expected, it is evident that the propulsion system's response to positive and negative step inputs of the same magnitude are asymmetrical. This asymmetry can be primarily attributed to the lack of active braking of the angular momentum, along with the unidirectional drag torque.

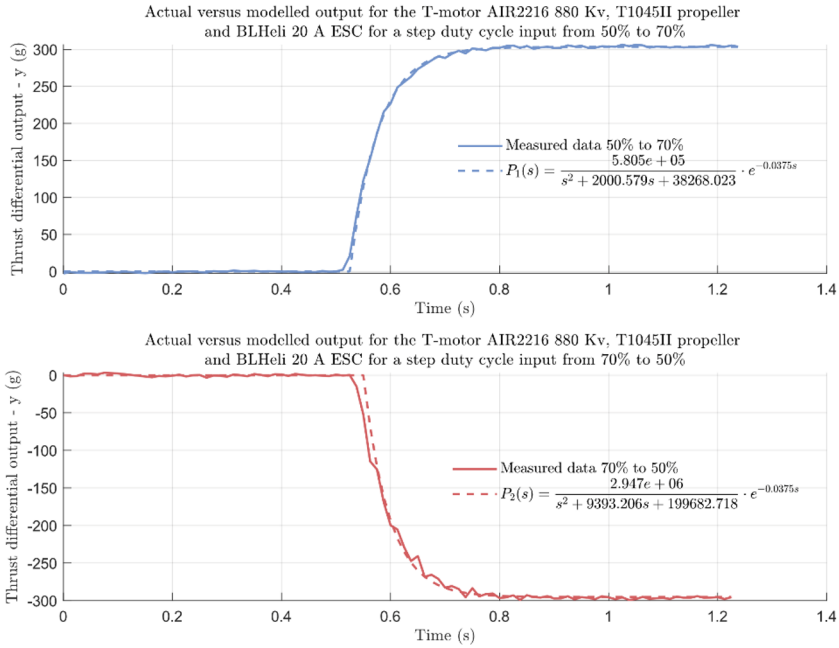

Fig. 13. Dynamic response tests for an example step-up and step-down input on the Holybro X500 propulsion system

Table 6. Dynamic response model characteristics for the step-up and step-down tests shown in Fig. 13.

Parameter	ω_n (rad/s)	ζ	τ (s)	Fit to estimation data	RMSE (g)
50% to 70% step test	195.62	10.22	0.0375	97.9%	3.04
70% to 50% step test	446.88	21.02	0.0375	94.4%	7.96

The measurement rig's design files and code base, along with a collection of static and dynamic tests of varying propulsion systems are made to be openly available [16].

4 Conclusion

The Propulsion Rig is a low-cost and open-source platform capable of measuring performance data of small- to medium-sized multirotor propulsion systems. The data can be used to inform and generate fundamental models of the multirotor propulsion system. This allows for conceptual designs to be experimentally validated. Additionally, once the propulsion system is selected, the associated model can be incorporated into the control scheme of the multirotor, thereby improving the performance and stability of the multirotor. Through experimentation and error analysis, static performance data acquired from the rig is proven to be comparable to reputable online data. All items scoped within the user requirement specifications have been achieved, and all aspects of this project are publicly available on GitHub, including the database of propulsion system tests [16].

Future work may explore three avenues to develop and improve the measurement rig. Firstly, the HX711 (ADC and amplifier) currently limits the sampling rate, and if replaced, would allow for significantly greater embedded system sampling rates. Secondly, the two microcontrollers employed can be replaced with a readily available, low-cost microcontroller that is capable of multi-threading, such as suitable EPS-32. Lastly, the measurement rig's instrumentation can be packaged into a single PCBA, thereby creating a plug-and-play solution.

References

[1] Tyto Robotics, Series 1585 Thrust Stand (2025). URL: https://www.tytorobotics.com/pages/series-1580-1585
[2] Foxtech, LY-10KGF Thrust Stand (2025). URL: https://store.foxtech.com/ly-10kgf-thrust-stand/?srsltid=AfmBOoqZxbrQAtg7qbx_vJ_zT88jPSkuofQY0Ntf4Ixf3xx8XBCA_pDH
[3] Wing Flying Technologies, LY-10KGF Thrust Stand (2025). URL : https://www.wingflyingtech.com/motor-test/Drone-Test-Equipment.html
[4] G.G. Neto, Model identification of a brushless DC motor and propeller for multicopter applications, Master Thesis, Politecnico di Milano, Dipartimento di Elettronica, Informazione e Bioingegneria, 2019
[5] A. Brezina, S. Thomas, Measurement of static and dynamic performance characteristics of electric propulsion systems, in Proceedings of the 51st AIAA Aerospace Sciences Meeting including the New Horizons Forum and Aerospace Exposition, Grapevine, Texas, United States of America, January 7-10 (2013), p. 500. https://doi.org/10.2514/6.2013-500
[6] J. Buzzatto, M. Liarokapis, A Benchmarking Platform and a Control Allocation Method for Improving the Efficiency of Coaxial Rotor Systems. IEEE Robot. Autom. Lett. **7**, 5302 (2022). https://doi.org/10.1109/LRA.2022.3153999
[7] TE Connectivity, COMPRESSION LOAD CELL-100/150MV/.5-4.5V (2025). URL : https://www.te.com/en/product-CAT-FSE0001.html
[8] Transducer Techniques, RTS-25 Reaction Torque Sensor (2025). URL: https://www.transducertechniques.com/rts-25-reaction-torque-sensor.aspx
[9] National Instruments, NI myRIO-1900 (2025). URL: https://us.testforce.com/myrio-for-academic-customers-only.html
[10] N. Bartnick, Brushless Motor Thrust Stand (2025). URL: https://www.instructables.com/Brushless-Motor-Thrust-Stand/
[11] Dassault Systèmes - SolidWorks Corporation, SolidWorks Simulation (2025). URL: https://www.solidworks.com/product/solidworks-simulation
[12] Dassault Systèmes - SolidWorks Corporation, SolidWorks Simulation (2025). URL : https://www.solidworks.com/product/solidworks-simulation
[13] DIYElectronics, Infrared Obstacle Avoidance Proximity Sensor Module FC-51 (2025). URL: https://www.diyelectronics.co.za/store/ir/1294-infrared-obstacle-avoidance-proximity-sensor-module-fc-51.html
[14] Allegro MicroSystems, Thermally Enhanced, Fully Integrated, Hall-Effect-Based Linear Current Sensor IC with 100 μΩ Current Conductor (2025). URL: https://www.allegromicro.com/~/media/files/datasheets/acs758-datasheet.ashx
[15] SparkFun Electronics, PARALLEL BEAM LOAD CELL (2025). URL: https://cdn.sparkfun.com/datasheets/Sensors/ForceFlex/TAL220M4M5Update.pdf
[16] GitHub, AltAirCoaxialVariableTiltMRAV/Propulsion-Rig (2025). URL: https://github.com/AltAirCoaxialVariableTiltMRAV/Propulsion-Rig